Concentration of Ce^{3+} and Oxygen Vacancies in Cerium Oxide Nanoparticles

P. Dutta, S. Pal, and M. S. Seehra*

Department of Physics, West Virginia University, Morgantown, West Virginia 26506-6315

Y. Shi, E. M. Eyring, and R. D. Ernst

Department of Chemistry, University of Utah, Salt Lake City, Utah 84112

Received July 10, 2006. Revised Manuscript Received August 29, 2006

Temperature variations of the electron magnetic resonance (EMR) spectra and magnetization measurements are used to show that Ce^{3+} ions in concentration ≃18% are present in 3 nm CeO_2 nanoparticles supported on silica aerogel. It is argued that the presence of Ce^{3+} implies the defect structure CeO_{2-x} for ceria nanoparticles due to oxygen vacancies. This transformation of Ce^{4+} to Ce^{3+} driven by oxygen vacancies may be the key to understanding the catalytic properties of ceria.

Introduction

Ceria is an important support material for catalysts used in a variety of industrially useful processes such as automotive catalytic converters, water−gas shift (WGS) reactions at lower temperatures, fuel cells, and production and purification of hydrogen.[1−4] Recently, Esch et al.[5] used high-resolution scanning tunneling microscopy to show that the surface of ceria (CeO_2) contains oxygen vacancies, leaving electrons which may reduce Ce^{4+} present in CeO_2 to Ce^{3+} in CeO_{2-x}. The presence of highly mobile lattice oxygen available at the surface of ceria is, therefore, probably responsible for the useful catalytic properties of ceria. Since the effective ionic radius of Ce^{3+} is about 14% larger than that of Ce^{4+} in the same coordination,[6] the size dependence of the lattice parameter observed in ceria nanoparticles (NP) has also been used recently to imply the presence of Ce^{3+}.[7−9] Other techniques reported recently for determining the Ce^{3+}/Ce^{4+} concentrations are XPS (X-ray photoelectron spectroscopy) in ceria nanoparticles[9,10] and XANES (X-ray absorption near edge spectroscopy) in $Ce_{1-x}Zr_xO_{2-y}$.[11] Of these two techniques, XPS has been shown to overestimate the Ce^{3+} concentration.[10]

In this paper, we have used magnetic methods to provide convincing and direct evidence for the presence of Ce^{3+} ions in 3 nm ceria NP from the temperature variations of the electron magnetic resonance (EMR) spectra associated with Ce^{3+} ions. Additional confirmation and concentration of Ce^{3+} ions is obtained from the temperature and magnetic field variations of the magnetization. The concentration of Ce^{3+} ions in our 3 nm ceria NP supported on silica aerogel is determined to be about 18% from both techniques.

For stoichiometric CeO_2, the electronic state of Ce is Ce^{4+} which is diamagnetic and hence EMR silent. For Ce^{3+}, the electronic state is $f^1\ {}^2F_{5/2}$ with spin $S = {}^1/_2$ and the total angular momentum $J = {}^5/_2$. Studies of Ce^{3+} doped in single crystals of ethyl sulfate[12] and strontium barium niobate[13] have described the effect of crystalline field (CF) on the Ce^{3+} energy levels. In axial CF, the $J = {}^5/_2$ state splits into three Kramer doublets with $J_Z = \pm{}^1/_2$, $\pm{}^5/_2$, and $\pm{}^3/_2$, in order of increasing energy. Therefore, the role of these states in the observed EMR spectra and magnetization studies can be used to unambiguously identify Ce^{3+} and determine its concentration. This is the procedure followed in the present work.

Sample Preparation

The sample of 10% ceria/silica aerogel was prepared at the University of Utah where ceria was loaded onto the prepared silica alcogel[14] in the following way. The silica alcogel (10 mL, 545 mg of SiO_2) was exchanged with a THF (tetrahydrofuran) solution (30 mL) of $Ce_2(O^iPr)_8(^iPrOH)_2$ (755 mg). After approximately 2−3 days to equilibrate, the concentration was such that the alcogel would be 10% ceria (w/w). Subsequently, the alcogel was dried via supercritical CO_2. The alcogel was transferred to an autoclave and was exchanged with liquid CO_2 for 4−5 h at a temperature of

* Corresponding author. E-mail: mseehra@wvu.edu.

(1) Park, S.; Vohs, J. M.; Gorte, R. J. *Nature* **2000**, *404*, 265.
(2) Fu, Q.; Saltsburg, H.; Flutzani-Stephanopoulos, M. *Science* **2003**, *301*, 935.
(3) Otsuka, K.; Ushiyama, T.; Yamanaka, I. *Chem. Lett.* **1993**, *9*, 1517.
(4) Deluga, G. A.; Salge, S. R.; Schmidt, L. D.; Verykios, X. E. *Science* **2004**, *303*, 993.
(5) Esch, F.; Fabris, S.; Zhou, L.; L. Montini, L.; Africh, C.; Fornasiero, P.; Comelli, G.; Rosie, R. *Science* **2005**, *309*, 752.
(6) Shannon, R. D. *Acta Crystallogr.* **1976**, *A32*, 751.
(7) Tsunekawa, S.; Ishikawa, K.; Li, Z.-Q.; Kawazoe, Y.; Kasuya, A. *Phys. Rev. Lett.* **2000**, *85*, 3440.
(8) Zhang, F.; Chan, S.; Spanier, J. E.; Apak, E.; Jin, Q.; Robinson, R. D.; Herman, I. P. *Appl. Phys. Lett.* **2002**, *80*, 127.
(9) Deshpande, S.; Patil, S.; Kuchibhatla, S.; Seal, S. *Appl. Phys. Lett.* **2005**, *87*, 133113.
(10) Zhang, F.; Wang, P.; Koberstein, J.; Khalid, S.; Chan, S.-W. *Surf. Sci.* **2004**, *563*, 74.
(11) Zhang, F.; Chen, C. H.; Raitano, J. M.; Hanson, J. C.; Caliebe, W. A.; Khalid, S.; Chan, S.-W. *J. Appl. Phys.* **2006**, *99*, 084313.
(12) Scott, P. L.; Jeffries, C. D. *Phys. Rev.* **1962**, *127*, 32.
(13) Wingbermuhle, J.; Meyer, M.; Schirmer, O. F.; Pankrath, R.; Kremer, R. K. *J. Phys. Condens. Matter* **2000**, *12*, 4277.
(14) Dunn, B. C.; Cole, P.; Covington, D.; Webster, M. C.; Pugmire, R. J.; Ernst, R. D.; Eyring, E. M.; Shah, N.; Huffman, G. P. *Appl. Catal., A* **2005**, *278*, 233.

10.1021/cm061580n CCC: $33.50
Published on Web 09/26/2006

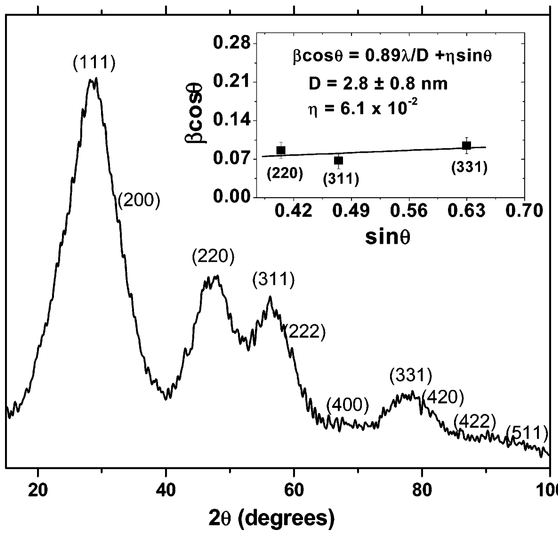

Figure 1. Room-temperature X-ray diffraction pattern of CeO_2/silica aerogel. The miller indices (*hkl*) correspond to tetragonal CeO_2. In the inset, the plot of $\beta \cos \theta$ vs $\sin \theta$ is shown to yield the particle size $D \simeq 2.8$ nm.

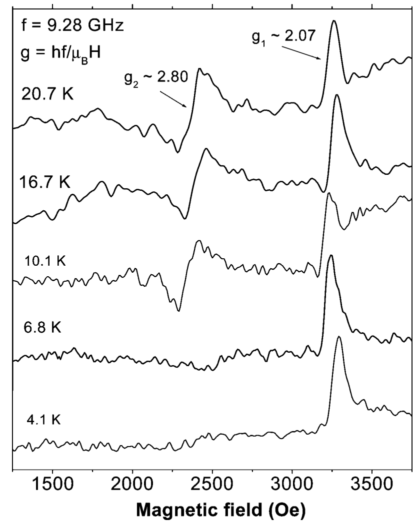

Figure 2. EMR spectra for the ceria NP for selected temperatures shown. Note the first appearance of the $g = 2.80$ line near 10 K, which is crucial for identifying Ce^{3+}.

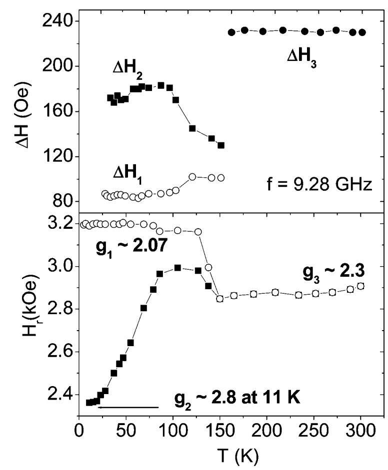

Figure 3. Temperature variation of the resonance field H_r and line width ΔH for the observed EMR lines. Note merging of the two lines for $T > 150$ K, where ΔH_3 nearly equals $\Delta H_1 + \Delta H_2$.

28 °C and with dynamic venting of the liquid CO_2 and residual THF. After the exchange, the system was heated to beyond supercritical conditions (50 °C, 1300−2000 psi). The supercritical CO_2 was vented in a controlled fashion, over 1−2 h, to yield aerogel doped with a cerium isopropoxide complex. The aerogel was sieved (<45 mesh) and was calcined (air, 5 °C/min ramp, 450 °C, 4 h soak) to yield aerogel doped with ceria.

Results and Discussion

All the observed lines in the XRD spectra of the above prepared 10% ceria/90% aerogel (using Cu Kα radiation with $\lambda = 0.154185$ nm) can be identified with cubic CeO_2 (Figure 1). The width β of the various Bragg lines (after correcting for the instrumental width) is fitted to the modified Scherrer equation: $\beta \cos \theta = (0.89\lambda/D) + \eta \sin \theta$,[15] where η is the strain and D is the size of the NP. The plot of $\beta \cos \theta$ versus $\sin \theta$ for the reasonably well-resolved Bragg lines (220), (311), and (331) is shown in the inset of Figure 1. The slope of the fit yields the strain $\eta = 6.1 \times 10^{-2}$ and the intercept at $\sin \theta = 0$ equals 0.51 and gives the particle size $D = 2.8 \pm 0.8$ nm. Transmission electron microscopy (not shown) confirmed this particle size. The EMR measurements at frequency $f = 9.28$ GHz were carried out in the temperature range of 4−300 K using a conventional X-band spectrometer and a variable temperature cryostat. The measurements of the magnetization M vs applied field H and temperature T were carried out using a commercial SQUID (superconducting quantum interference device) magnetometer.

The EMR spectra are strongly temperature-dependent (Figure 2). At 4.1 K, only a single line with $g = 2.07$ is observed where $g = hf/\mu_B H_r$ with h being Planck's constant, μ_B the Bohr magneton, and H_r the resonance field. As T is raised, a second line at lower H_r with $g = 2.80$ is observed above ≈10 K. The temperature dependence of H_r and the line width ΔH for the two lines is shown in Figure 3. Interestingly, near 150 K, these two lines merge into a single line with $g \approx 2.30$ with line width ΔH nearly equal to the sum of the line widths of the two lines (Figure 3). With use of the discussion given earlier for three Kramer doublets of Ce^{3+} ions, the line with $g = 2.07$ is associated with the $J_z = \pm^1/_2$ level and the line at $g = 2.80$ with the $J_z = \pm^5/_2$ state separated from the ground state by energy $T_1 = 10$ K, whereas the $J_z = \pm^3/_2$ level lies $T_2 = 150$ K above the ground state level of $J_z = \pm^1/_2$. Although g values of Ce^{3+} are highly anisotropic as observed in single crystals,[12,13] in polycrystalline samples only a single line due to the most prominent g component is often observed.[16] For $T \geq 150$ K, when the $J_z = \pm^3/_2$ also gets sufficiently populated, the EMR lines from all three Kramer doublets merge into a single line at $g = 2.30$. On the other hand, for $T < 10$ K, only the $J_z = \pm^1/_2$ is sufficiently populated, yielding only the $g = 2.07$ line. The energy splitting of 10 and 150 K observed here for Ce^{3+} ions in CeO_{2-x} are quite similar to those reported

(15) See, e.g., Dutta, P.; Manivannan, A.; Seehra, M. S.; Shah, N.; Huffman, G. P. *Phys. Rev. B* **2004**, *70*, 174428.

(16) Canevali, C.; Mattoni, M.; Morazzoni, F.; Scotti, R.; Casu, M.; Musinu, A.; Krsmanovic, R.; Polizzi, S.; Speghini, A.; Bettinelli, M. *J. Am. Chem. Soc.* **2005**, *127*, 14681.

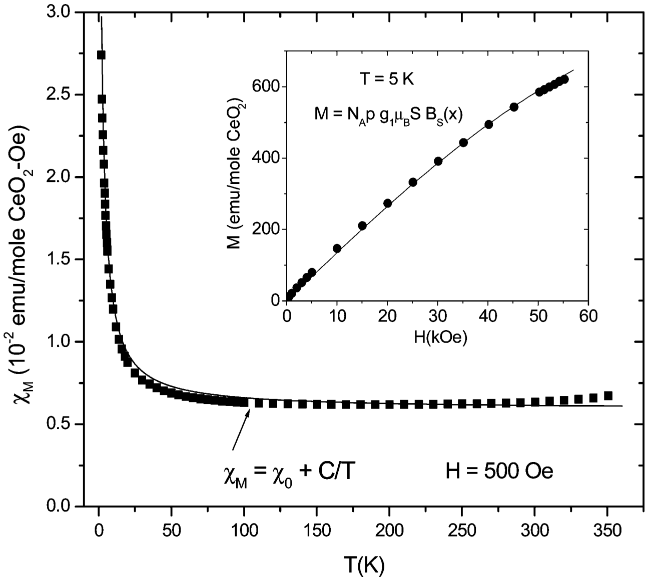

Figure 4. Temperature variation of the magnetic susceptibility χ_M measured at $H = 500$ Oe. The solid line is the Curie law fit with $\chi_0 = 5.9 \times 10^{-3}$ emu/mol of CeO_2•Oe and $C = 7.2 \times 10^{-2}$ emu K/mol of CeO_2•Oe. In the inset, the plot of M vs H at $T = 5$ K is shown, with the solid line fit to eq 2 discussed in the text.

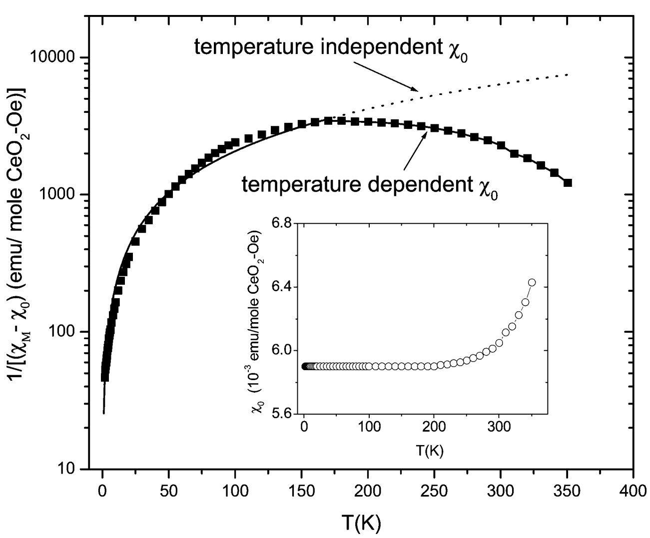

Figure 5. Plot of $(\chi_M - \chi_0)^{-1}$ vs T to demonstrate the departures from the Curie law variation. The dotted (solid) line is fit to eq 1 with temperature-independent (temperature-dependent) χ_0. The inset shows χ_0 used in the fit (solid line).

for Ce^{3+}/ethyl sulfate.[12] The axial crystal field for Ce^{3+} in CeO_{2-x} nanoparticles due to oxygen vacancies is discussed in ref 9.

To further test the above model, we next analyze the data of magnetic susceptibility $\chi = M/H$ ($H = 500$ Oe) versus T shown in Figure 4. Although the data fit approximately the Curie law variation $\chi_M = \chi_0 + C/T$ at lower temperatures, a more detailed analysis is possible by plotting $(\chi_M - \chi_0)^{-1}$ versus T (Figure 5) where deviations from the Curie law at higher temperatures are clearly evident. Here, χ_0 includes contributions from the diamagnetic susceptibility χ_d and the Van Vleck susceptibility χ_{VV}, which may increase at higher temperatures because of the thermal expansion of the lattice.[17]

With use of the energy levels of the three Kramer doublets with energy splitting of T_1 and T_2 from the ground level, the calculated susceptibility $(\chi_M - \chi_0)$ can be shown to equal[18]

$$(\chi_M - \chi_0) = \frac{N_A p g_1^{\,2} \mu_B^{\,2}}{4kT}\left\{\frac{1 + \alpha_1 e^{-T_1/T} + \alpha_2 e^{-T_2/T}}{1 + e^{-T_1/T} + e^{-T_2/T}}\right\} \quad (1)$$

where $\alpha_1 = (g_2/g_1)^2$, $\alpha_2 = (g_3/g_1)^2$, k is the Boltzmann constant, p is the concentration of Ce^{3+} ions, and N_A is Avogadro's number. With use of $g_1 = 2.07$, $g_2 = 2.80$, $g_3 = 2.30$, $T_1 = 10$ K, $T_2 = 150$ K, and $p = 0.18$, the calculated $(\chi_M - \chi_0)^{-1}$ vs T is shown as a dotted line in Figure 5 for temperature-independent $\chi_0 = 5.9 \times 10^{-3}$ emu/mol of CeO_2•Oe. To improve the agreement above 200 K, a temperature dependence for χ_0 above 200 K is inferred, which can result from the thermal expansion of the lattice.[17] The solid line in Figure 5 is the fit to eq 1 with some temperature dependence to χ_0 above 200 K shown in the inset of Figure 5.

At 5 K, only the ground state level with $J_z = \pm 1/2$ is sufficiently populated. The M versus H data then should follow the Brillouin function:

$$M = N_A p g_1 \mu_B S B_S(x) \quad (2)$$

where $x = g_1\mu_B HS/kT$, $S = 1/2$, and $B_S(x) = [(2S + 1)/2S] \coth(2S + 1)x/2S - (1/2S) \coth x/2S$.

In the inset of Figure 4, the comparison of the data with the calculated M from eq 2 using $p = 0.18$ shows very good agreement. Thus, the magnitude of p determined from both the M versus T and M versus H variations are identical (within $\pm 5\%$), providing additional confidence for our conclusion about the identification of $Ce^{3+}$and its concentration.

Conclusion

In summary, careful analysis of the temperature dependence of the EMR spectra and magnetic susceptibility leads to the identification of Ce^{3+} and determine its concentration in CeO_2 NP. As discussed in other publications,[5,7–9] the presence of Ce^{3+} is a result of oxygen vacancies and this effect is enhanced in NP because a larger fraction of the atoms are on the surface as the particle size is reduced and the surface atoms have reduced coordination. This leads to CeO_{2-x} as the structure for ceria NP. The oxygen vacancies lead to the transformation $Ce^{4+} \rightleftarrows Ce^{3+}$, which may be at the heart of the many useful properties of ceria NP mentioned earlier in the paper.

Acknowledgment. Financial support for this research, provided by the U.S. Department of Energy (Contract # DE-FC26-05NT42456), is gratefully acknowledged.

CM061580N

(17) Burgardt, P.; Seehra, M. S. *Solid State Commun.* **1977**, *22*, 153.

(18) For example, see Gordon, B. L.; Seehra, M. S. *Phys. Rev. B* **1989**, *40*, 2348, for the procedure to derive the expression for χ from a known energy level diagram.